Supplementary Materials

Rare-earth-cation effects in $CuO/Ln_2Ce_2O_7$ catalysts for methanol steam reforming

Tingting Zhang[1], Xin Liu[1], Xinran Pang[1], Yiyun Ke[1], Junwei Xu[2,*], Jiamei Ma[1,*], Xiang Wang[1,*]

[1]Key Laboratory of Jiangxi Province for Environment and Energy Catalysis, School of Chemistry and Chemical Engineering, Nanchang University, Nanchang 330031, Jiangxi, China.
[2]Jiangxi Academy of Sciences, Nanchang 330096, Jiangxi, China.

[*]**Correspondence to:** Dr. Jiamei Ma, Jiangxi Academy of Sciences, Nanchang 330096, Jiangxi, China. E-mail: majiamei@ncu.edu.cn; Dr. Junwei Xu, Prof. Xiang Wang, Key Laboratory of Jiangxi Province for Environment and Energy Catalysis, School of Chemistry and Chemical Engineering, Nanchang University, Nanchang 330031, Jiangxi, China. E-mail: xujunwei@email.ncu.edu.cn; xwang23@ncu.edu.cn

Details of catalytic characterizations

XRD: The powder X-ray diffraction (XRD) patterns were collected on a Bruker AXS D8 focused X-ray diffractometer with Cu Kα radiation at 40 kV and 30 mA, with the 2θ scanning angel of 10° to 80° and a scanning speed of $10^o \cdot min^{-1}$.

ICP-OES: The actual contents of Cu in the catalysts were quantitatively analyzed by inductively coupled plasma-atomic emission spectroscopy on an ICP-OES instrument (Varian 715-ES) manufactured in the United States.

Raman: Raman spectra were recorded on a Renishaw Invia Raman spectrometer manufactured in the United Kingdom, equipped with a 532 nm argon laser excitation source and a Renishaw RenCam CCD detector.

TEM images and elemental mapping images: Transmission electron microscopy (TEM) images and elemental mapping images were obtained to visualize the morphology and nanostructure of catalysts by FEI-Tecnai G2 F30 (USA).

N_2 adsorption-desorption: The texture properties of the samples were measured by N_2 adsorption-desorption at 77 K on an ASAP2020 instrument. The specific surface areas of the catalysts were calculated by a BET method, and the pore volume together with pore size distribution were quantified with a BJH method.

X-ray photon spectroscopic (XPS): X-ray photon spectroscopic (XPS) spectra of the samples were obtained on an RBD upgraded PHI-5000C ESCA apparatus using the Mg Kα irradiation source (operated at 250 W and 14 kV). The standard C 1s signal at a binding energy (BE) of 284.6 eV was used as the reference for BE calibration.

H_2-TPR: H_2-TPR experiments were carried out on FINESORB 3010C instrument. Generally, 50 mg catalysts were used for the tests. Before the experiments, the catalysts were pretreated in a high purity air flow at 400 °C for 30 min to remove preformed surface carbonates and any possible impurities. After purging with an ultra-high purity Ar flow at room temperature for 30 min, the temperature was then increased from room temperature to 600 °C with a ramp of 10 $^oC \cdot min^{-1}$ in a 30 $mL \cdot min^{-1}$, 10% H_2/Ar gas mixture flow. A thermal conductivity detector (TCD) was employed to monitor the H_2 uptake. To quantify the H_2 consumption amount, a 99.99% CuO sample was used as the calibration standard.

CO_2-TPD: CO_2-TPD analyses were carried out on a Micromeritics ASAP2920 instrument. 50 mg catalysts were treated first for 1 h at 400 °C in a He flow, followed by cooling to 50 °C, and then saturated in a 30 $mL \cdot min^{-1}$ CO_2 flow at 50 ^oC for 1 h. After CO_2 chemisorption, the sample was flushed for 30 min in a flow of 30 $mL \cdot min^{-1}$ 99.99% He to get rid of any physically adsorbed CO_2. Subsequently, the CO_2-TPD was started from 50 °C to 800 °C with heating ramp of 10 $°C \cdot min^{-1}$ in still the 99.99% He flow. A TCD detector was used to analyze the desorbed CO_2. The CO_2 desorption amount was quantified by using a $MgCO_3$ (99.9%) standard, which decomposes completely around 600 °C according to the stoichiometric equation of $MgCO_3 = MgO$

+ CO_2. The reaction products, including CO (m/z= 28) and CO_2 (m/z= 44) were monitored by the MS detector.

Cu dispersion: The dispersion and specific surface area of Cu in different catalysts were determined by N_2O titration on FINESORB 3010C instrument equipped with a TCD. Typically, 50 mg calcined sample was weighed for testing. In detail, the sample was purged by an Ar (99.99%) flow for 60 min to cleanse its surface. Afterward dropping to 50 °C, the temperature was increased to 400 °C to reduce the original CuO into metallic Cu in a flow of 10 vol% H_2/Ar, and the H_2 consumption amount (X) was quantified. The sample was then cooled to 30 °C, which was followed by purging with Ar to remove any physically adsorbed H_2. Afterwards, the surface metallic Cu was re-oxidized to Cu_2O in a 1000 ppm N_2O/Ar flow (20 mL·min^{-1}) for 20 min. Finally, the flow was switched back to the 10 vol% H_2/Ar feed with the temperature being raised to 400 °C at a rate of 10 °C·min^{-1}. In this way, the H_2 consumption amount (Y) corresponding to the reduction of surface Cu_2O was quantified. Assuming a catalyst surface is fully covered by Cu atoms, its density should be 1.4×10^{19} copper atoms·m^{-2}. Based on this, the dispersion degree, active surface area and particle size of metallic Cu are calculated with equation (1) and (2), respectively.

Dispersion degree: $D = \frac{2Y}{X} \times 100\%$ (1)

Specific copper active area: $S = \frac{2Y \times N_{av}}{X \times M_{Cu} \times 1.4 \times 10^{19}} \approx \frac{1353Y}{X} \left({}^{m^2\ Cu}/_{g\ Cu} \right)$ (2)

***In-situ* DRIFTS:** *In-situ* DRIFTS experiments were performed on a Bruker FTIR spectrometer equipped with a MCT detector cooled by liquid nitrogen. To investigate the pathway of methanol steam reforming for hydrogen production. The operational procedures are as follows: The catalyst was first reduced at 300 °C for 40 minutes in a 10% H_2/Ar atmosphere with a flow rate of 30 mL/min. It was then purged with Ar (30 mL/min) for 1 hour and cooled to 50 °C for background spectrum collection. Pure methanol vapor was introduced into the reaction cell using Ar, and the temperature was increased to 400 °C at a rate of 10 °C/min, followed by a 40-minute reaction period during which *in-situ* infrared signals were collected. The system was then

switched to a CH_3OH/H_2O mixed vapor with a molar ratio of 1:1.5. After purging with Ar for 1 hour at 400 °C, the temperature was reduced to 50 °C for background spectrum collection. The mixed vapor was then introduced into the reaction cell with Ar, and the temperature was raised to 300 °C at the same heating rate. A 60-minute reaction period followed, after which *in-situ* infrared signals were again collected.

$^{18}O_2$-TPSR: Before the experiment, an oxygen flow was introduced into the catalyst at 600 °C for 30 min, then switched to Ar and cooled to 150 °C for 15 min. Subsequently, $^{18}O_2$ isotope gas was continuously introduced and heated at a rate of 10 °C·min^{-1} to 500 °C. For the three oxygen types, $^{18}O_2$ (m/z =36), $^{16}O^{18}O$ (m/z = 34) and $^{16}O_2$ (m/z = 32) were monitored.

Supplementary result

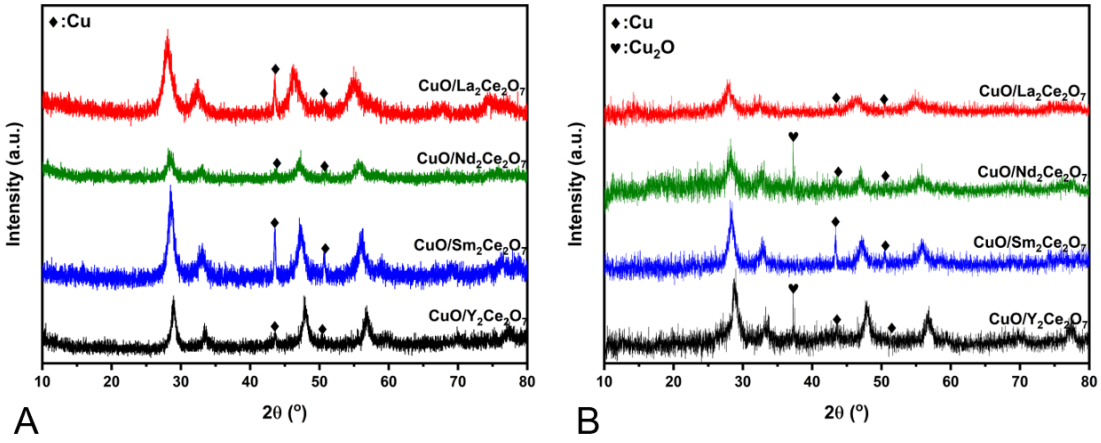

Supplementary Figure 1. A: XRD patterns of the reduced catalysts, B: XRD patterns of the spent catalysts.

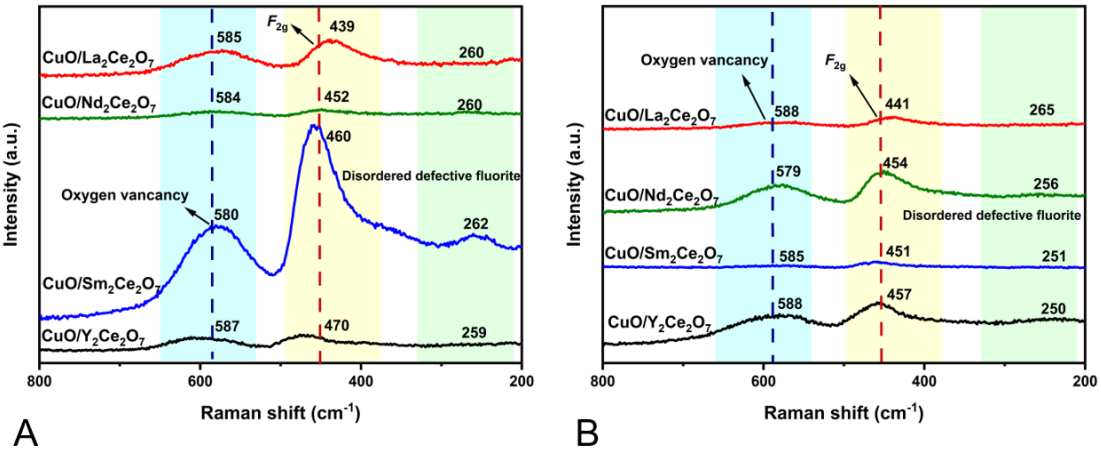

Supplementary Figure 2. A: Raman patterns of the reduced catalysts, B: Raman patterns of the spent catalysts.

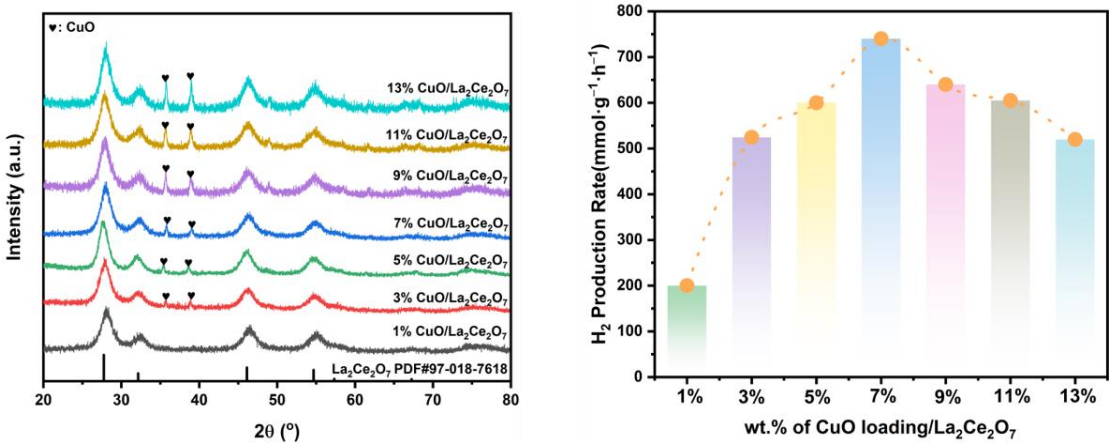

Supplementary Figure 3. $CuO/La_2Ce_2O_7$ catalysts with different CuO loading of 1, 3, 5, 7, 9, 11 and 13 wt.%: A: XRD patterns, B: H_2 production rates

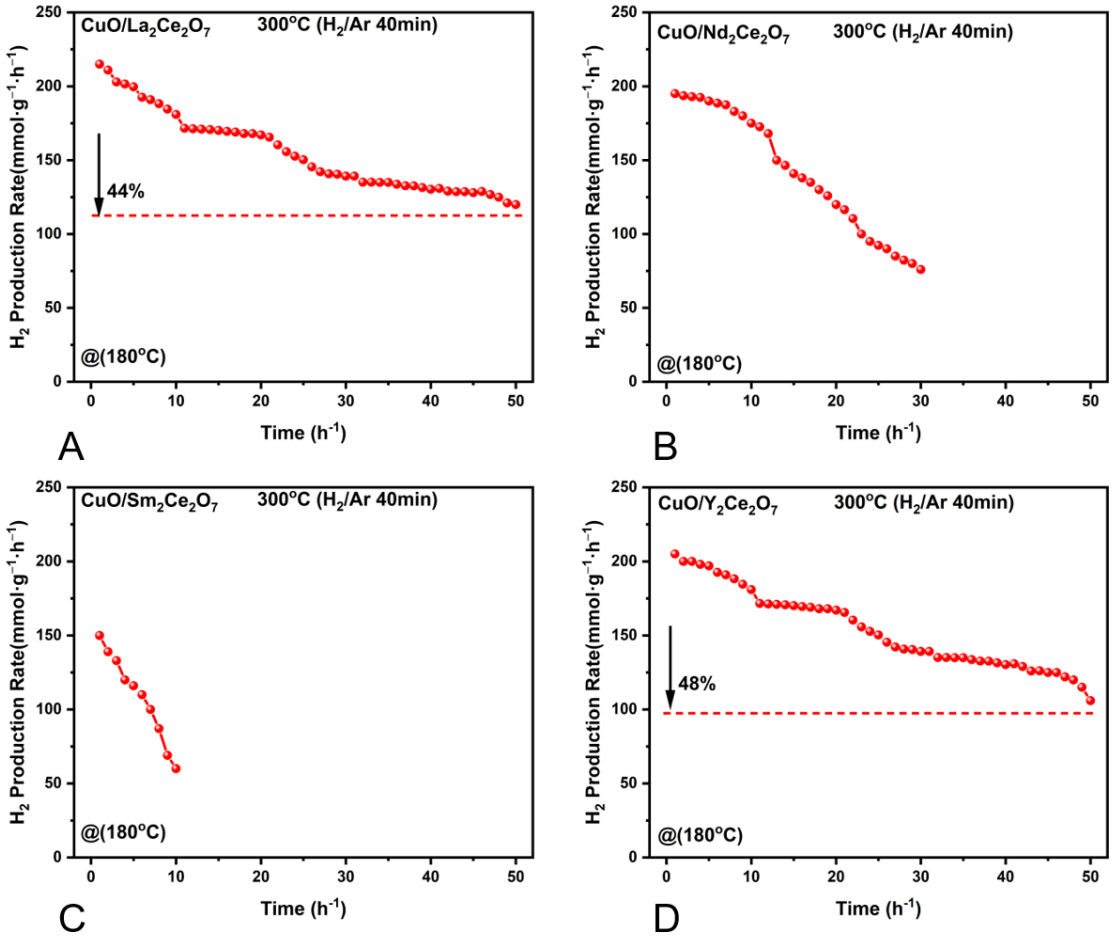

Supplementary Figure 4. H_2 production rate against time on stream over the catalysts at 180 ℃. A: $CuO/La_2Ce_2O_7$; B: $CuO/Nd_2Ce_2O_7$; C: $CuO/Sm_2Ce_2O_7$; D: $CuO/Y_2Ce_2O_7$.

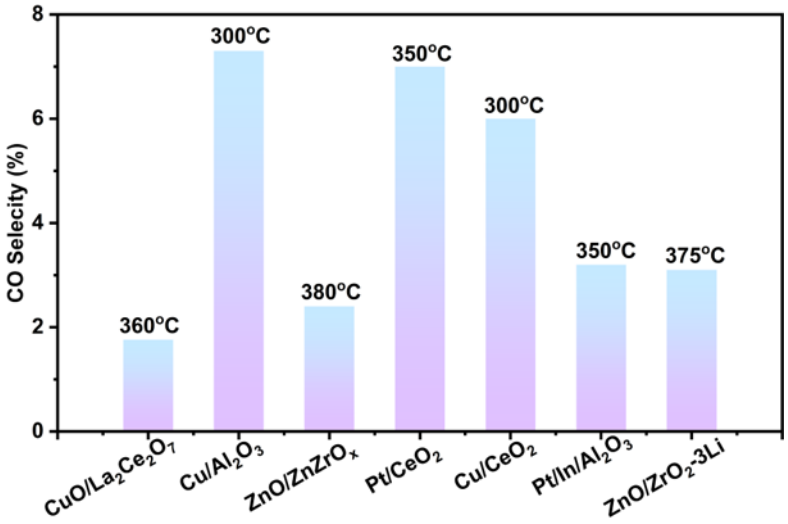

Supplementary Figure 5. Compare the reaction performance on $CuO/La_2Ce_2O_7$ with some reported typical catalysts[1-6].

Supplementary Table 1. Physical-chemical properties of the catalysts

Catalyst	Cu loading (wt.%)[a]	Specific surface area ($m^2 \cdot g^{-1}$)[b]		Pore volume ($cm^3 \cdot g^{-1}$)[b]		Pore size (nm)[b]	
		support	catalyst	support	catalyst	support	catalyst
$CuO/La_2Ce_2O_7$	6.8	39	30	0.17	0.12	3.02	4.16
$CuO/Nd_2Ce_2O_7$	6.8	18	17	0.06	0.03	3.41	4.16
$CuO/Sm_2Ce_2O_7$	6.8	7	5	0.06	0.02	4.45	4.48
$CuO/Y_2Ce_2O_7$	6.9	15	8	0.04	0.03	4.	3.43

a: ICP results; b: The results of N_2 adsorption-desorption.

As observed in Supplementary Table 1, the specific surface areas of the catalysts are smaller than that of the relative supports, which may be caused by the secondary calcination. Generally, the activity of the catalysts could be significantly influenced by their specific surface area and the distribution of Cu active sites, thereby promoting the adsorption of CH_3OH and H_2O. As presented in Table 1, the optimal catalyst $CuO/La_2Ce_2O_7$ possesses the largest specific surface area and highest Cu dispersion, which can certainly provide more active sites favorable to the reaction. Noteworthy,

this catalyst displays also the highest TOF among all the catalysts, testifying that it has the best intrinsic activity as well. This suggests that its performance advantage is not only determined by specific surface area or Cu dispersion degree but also stems more critically from the activity improvement of the individual active site.

Supplementary Table 2. Original kinetic data and linear fitting results for Arrhenius plots

Catalyst	Temperature (°C)	1000/T (K^{-1})	R_w (10^{-2} $mmol \cdot s^{-1} \cdot g^{-1}$)	TOF (h^{-1})
$CuO/La_2Ce_2O_7$	180	2.208	1.62	125
	190	2.159	2.16	167
	200	2.114	3.00	231
	210	2.067	4.26	329
$CuO/Nd_2Ce_2O_7$	180	2.208	0.5	53
	190	2.159	0.9	90
	200	2.114	1.3	133
	210	2.067	1.8	191
$CuO/Sm_2Ce_2O_7$	180	2.208	0.3	36
	190	2.159	0.4	59
	200	2.114	0.7	99
	210	2.067	1.3	168
$CuO/Y_2Ce_2O_7$	180	2.208	0.9	78
	190	2.159	1.3	112
	200	2.114	1.9	165
	210	2.067	2.7	239

Supplementary Table 3. Quantified H_2-TPR and CO_2-TPD results of the catalysts

Catalyst	H_2 uptake amount ($mmol \cdot g_{cat}^{-1}$) [a]	H/Cu atomic ratio [b]	Alkaline site amount (a.u.) [c]
$CuO/La_2Ce_2O_7$	1.30	2.00	100
$CuO/Nd_2Ce_2O_7$	0.93	1.70	44
$CuO/Sm_2Ce_2O_7$	0.75	1.37	15

$CuO/Y_2Ce_2O_7$	0.87	1.58	18

a: H_2-TPR results; b: Subtracting the H_2 consumption of the support; c: CO_2-TPD results.

REFERENCES

1. Y. Khani; N. Kamyar; F. Bahadoran; N. Safari. M. M. Amini. A520 MOF-derived alumina as unique support for hydrogen production from methanol steam reforming: The critical role of support on performance, *Renewable Energy*. 2020, 156, 1055-1064. DOI: https://doi.org/10.1016/j.renene.2020.04.136

2. X. Chen; J. Wang; Z. Han. et al. Methanol Steam Reforming over $ZnO/ZnZrO_x$: Performance Enhanced with a Cooperative Effect, *ChemCatChem*. 2022, 14, e202101232. DOI: https://doi.org/10.1002/cctc.202101232

3. V. Shanmugam; S. Neuberg; R. Zapf; H. Pennemann. G. Kolb. Hydrogen production over highly active Pt based catalyst coatings by steam reforming of methanol: Effect of support and co-support, *International Journal of Hydrogen Energy*. 2020, 45, 1658-1670. DOI: https://doi.org/10.1016/j.ijhydene.2019.11.015

4. F. Tonelli; O. Gorriz; A. Tarditi; L. Cornaglia; L. Arrúa. M. Cristina Abello. Activity and stability of a CuO/CeO_2 catalyst for methanol steam reforming, *International Journal of Hydrogen Energy*. 2015, 40, 13379-13387. DOI: https://doi.org/10.1016/j.ijhydene.2015.08.046

5. D. Liu; Y. Men; J. Wang. et al. Highly active and durable $Pt/In_2O_3/Al_2O_3$ catalysts in methanol steam reforming, *International Journal of Hydrogen Energy*. 2016, 41, 21990-21999. DOI: https://doi.org/10.1016/j.ijhydene.2016.08.184

6. Y. Wang; Y. Men; L. Liao. et al. Oxygen vacancy engineering in ZnO/ZrO_2 composite catalysts for highly enhanced hydrogen production by methanol steam reforming, *Colloids and Surfaces A: Physicochemical and Engineering Aspects*. 2024, 701, 134924. DOI: https://doi.org/10.1016/j.colsurfa.2024.134924